Electronic Supplementary Material (ESI) for ChemComm.

Design isolated iron species for Fenton reaction: lyophilization beat calcination treatment--Supporting Information

Leitao Zhang, Hui Ye, Lizhi Zhao, Lei Zhang, Lili Yao, Yuzhong Zhang*, and Hong Li

[*] Leitao Zhang, Hui Ye, Lizhi Zhao, Lei Zhang, Lili Yao, Prof. Yuzhong Zhang, Hong Li

State Key Laboratory of Separation Membranes and Membrane Processes, School of Materials Science and Engineering

Tianjin Polytechnic University, Tianjin, 300387 (P.R. China)

E-mail: zhangyz2004cn@vip.163.com

[**]This work is supported by the National Natural Science Foundation of China (No. 51503146, 51173132, 51373120, and 21204064), Science and Technology Commission Foundation of Tianjin (No.15JCZDJC37600, and 14JCQNJC03900), Public science and technology research funds projects of ocean (201305004-5), the Research Fund for the Doctoral Program of Higher Education (Funding No.20111201110003).

S1 Experimental Section

S1.1 Preparation of catalyst

10g 4A zeolite (Shanghai jiuzhou chemicals Co. Ltd, China) was added to 500mL 2000mg/L (pH≈1.67) $FeCl_3$ solution. After the mixture shaking for 3.5h and then ultrasonic treatment for 0.5h, the dark red solid (Fig. S1) could be obtained through vacuum filtration. In order to guarantee the complete rejection of the precursor, PVDF membrane (lab-made, 16%PVDF) was used as separation layer. Then the catalyst precursor was lyophilized at -55°C for different freezing time and these catalysts were named as F-55-X (X refers to the freezing time). In contrast, according to the literature[1], T500-6 and T350-6 was obtained through catalyst precursor incineration at 500°C or 350°C for 6h in air.

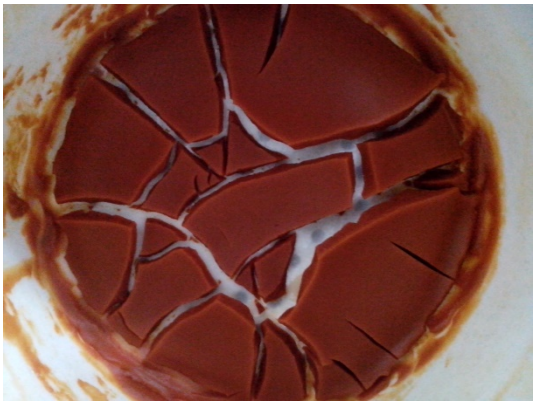

Fig. S1. The snapshot of catalyst precursor.

Table S1. The catalytic comparison in the presence different catalysts. Phenol=200 mg/L, 100 mL; H_2O_2/Phenol=12.75; Catalyst=0.1 g; Initial pH=2.00±0.01; T=25°C

Entry	Catalyst	Iron content (mM)	Time[a] (min)	Leaching[b] (Wt. %)	Leaching[c] (mg/L)
1	F-55-48 (0.10 g)	0.175 mM (8.90%)	13.5	1.14	1.12
2	F-55-34.5 (0.10g)	0.175 mM (8.90%)	15	0.68	0.67
3	F-55-24 (0.10g)	0.175 mM (8.90%)	13	0.75	0.74

4	T500-6 (0.10 g)	0.175 (8.90%)	mM	110	2.37	2.33
5	T350-6 (0.10 g)	0.175 (8.90%)	mM	45	4.04	3.97
6	$FeCl_3 \cdot 6H_2O$(0.10 g)	0.370 mM		100	100	all

[a] The time of phenol full degradation; [b] The ratio of leaching iron and total iron in catalysts; [c] The average iron-leaching during phenol degradation.

S1.2 Catalytic tests

100 mL of Milli-Q water containing 200 mg L^{-1} of phenol was placed in a 250 mL Erlenmeyer flask. The initial pH value was adjusted to defined values (Mettler-Toledo EL20K) by using 1M HCl and NaOH solution. Then 1 g/L corresponding catalyst was added, and the suspension was stirred for 80min to reach the balance of adsorption/ desorption and dispersion of catalyst. The reaction was triggered by the addition of H_2O_2 (50.57g/L, 2mL). Concentration of phenol and total iron were determined by 4-aminoantipyrite and 5- sulfosalicylic acid method, respectively. The determination of hydrogen peroxide was executed with potassium titanium (IV) oxalate.[2]

In the successive recycling experiments, catalysts were separated by centrifugation for 10min at 8000rpm and washed three times with Milli-Q water to remove the adsorbates. At initial pH=2.00, the phenol concentration in whole degradation process was detected. When the initial pH was set to 6.30, the reaction time was limited to 12h in each cycle.

S2 Characterization methods

XRD (X-ray diffraction) patterns were recorded using a BRUKER D8-DISCOVER X-ray diffractometer (Cu *Kα* radiation, λ=1.540598Å).

The morphology and structure were characterized using a field emission scanning electron microscope (FE-SEM, Rili S-4800, Japan) and a high resolution transmission electron microscope (HRTEM, Tecnai G2 F20, FEI). The TEM samples were prepared by milling the samples and dispersing in ethanol, which was then dropped onto the copper grid coated with carbon film.

The XPS (X-ray photoelectron spectroscopy) studies were carried with K-Alpha (Thermo Fisher Scientific, America), using an aluminum anode (Al Kα=1486.6 eV). The binding energy was referenced to the C1s peak at 284.8eV of the surface adventitious carbon.

The IR (Infrared radiation) spectra were recorded through a TENSOR37 spectrophotometer (Bruker AXS, USA).

The UV-Vis diffuse reflectance spectra measurements were performed on a Purkinje General TU-1901 spectrophotometer fitted with an integrating sphere. Diffuse reflectance spectra were recorded in air against $BaSO_4$.

N_2 adsorption-desorption isotherm was determined by Quantachrome NOVA 1000 Gas Sorption Analyzer and Micrometritics ASAP 2020 Physisorption Analyzer.

In phenol hydroxylation reaction, the reaction mixture was sampled periodically by syringe and analyzed by liquid chromatography (waters 2487) equipped with a Venusil C18 column. The mixture was separated on the column using a methanol/water mixture (60/40, volume ratio) as the mobile phase at a flow rate of 0.5 mL/min and detected at UV wavelength of 270nm.

The electron spin resonance (EPR) spectra in X-band (v≈9.5GHz) had been measured with a CW-spectrometer ELEXSYS 500 (Bruker) at a microwave power of 10mW, a modulation frequency of 100 kHz and a modulation amplitude of 0.5mT. The magnetic field was referenced according to the standard 2, 2-diphenyl-1-picrylhydrazyl-hydrate (DPPH). Measurements were made at 90K using commercial variable temperature control unit (Bruker) and a conventional EPR sample tube.

S3 Characterization of as-prepared catalysts

S3.1 XRD Characterization

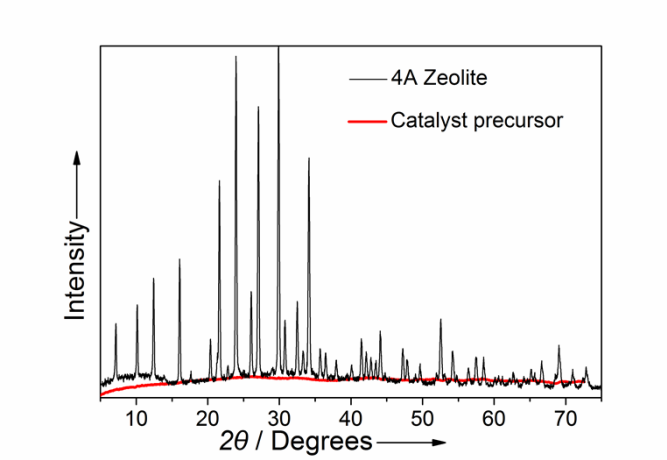

Fig. S2. XRD pattern of the 4A zeolite and catalyst precursor.

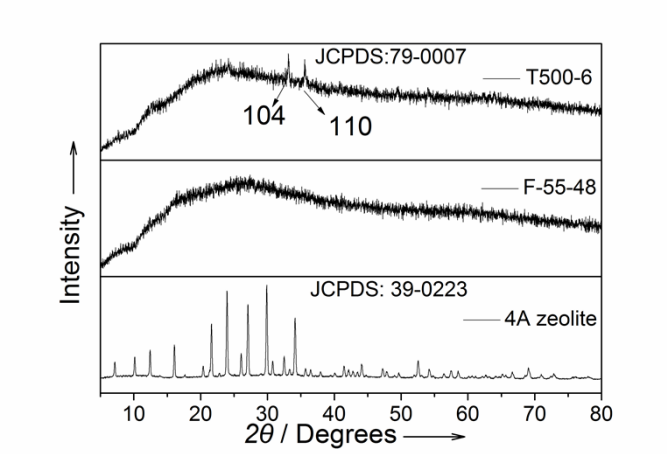

Fig. S3. XRD pattern of the 4A zeolite, F-55-48 and T500-6.

The crystallographic structure and purity of the as-prepared samples were examined by X-ray powder diffraction (XRD), and the results were presented in Fig. S2 and Fig. S3. 4A zeolite exhibited good crystalline structure (JPCDS no. 39-0223; space group Fm-3c a=b=c=24.555Å α=β=γ=90°), whereas the crystalline structure of catalyst precursor completely disappeared which was obtained through the mixing 4A zeolite and $FeCl_3$ solution in Fig. S2. As well, F-55-48 and T500-6 catalysts almost completely lost their diffraction peaks in Fig. S3. In addition, there were two diffraction peaks (33.14° (104) and 35.64° (110)) in good parallel with the characteristic signals of α-Fe_2O_3 (JPCDS no. 89-0598; space group R-3c a=b=5.038Å c=13.776Å α=β=90° γ=120°) crystal in T500-6 materials.

S3.2 SEM and TEM characterization

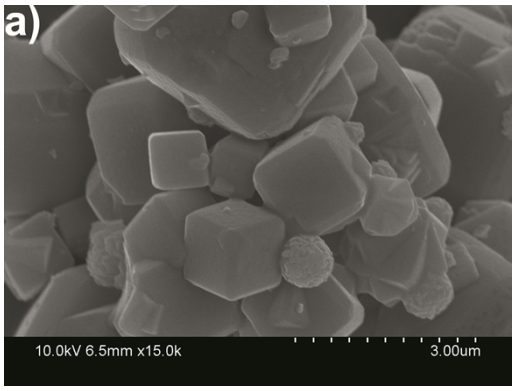

Fig. S4. SEM image of 4A zeolite

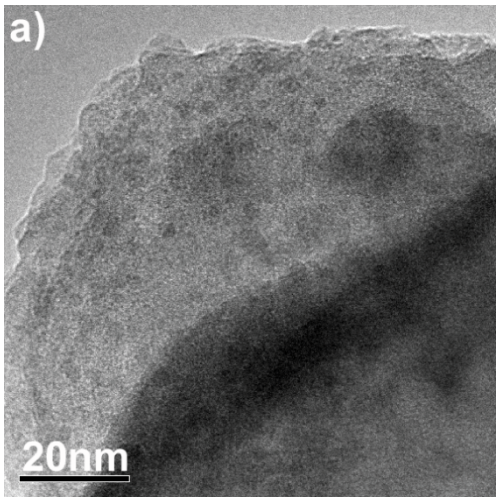

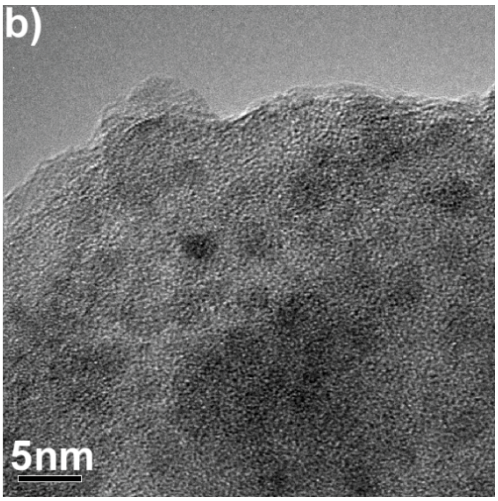

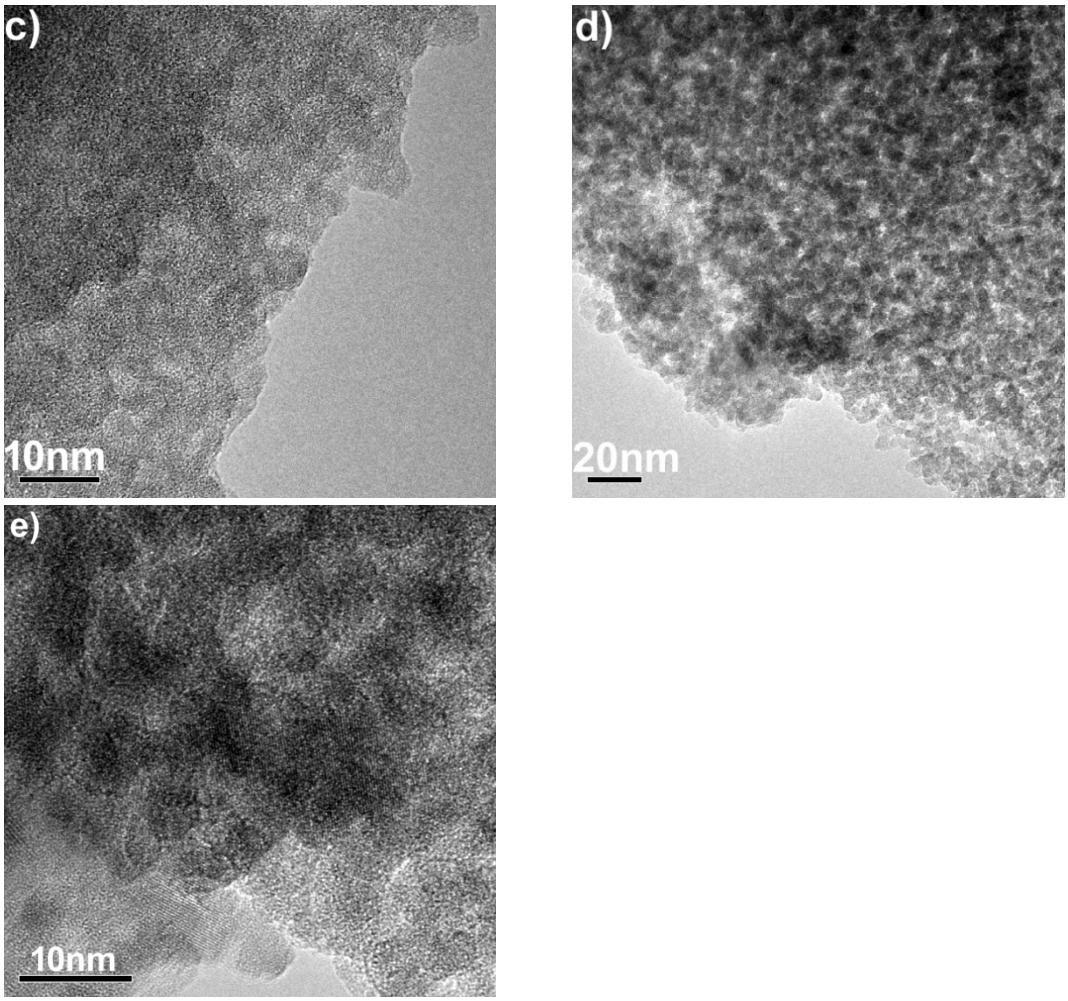

Fig. S5. TEM images of a, b, c) F-55-48; d, e) T500-6 samples.

S3.3 Fe $2p^{3/2}$ and $2p^{1/2}$ XPS characterization

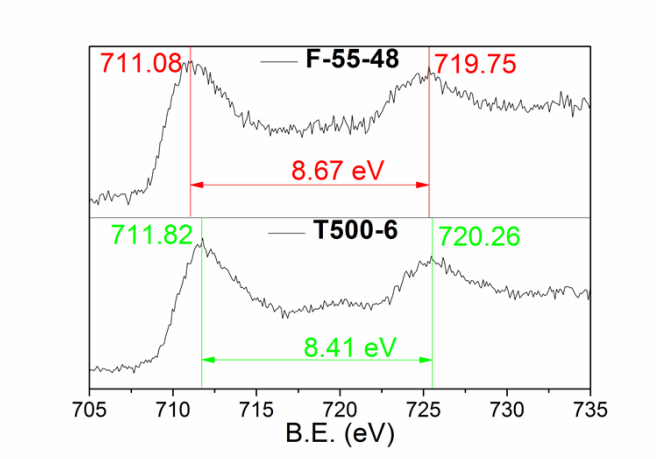

Fig. S6. Fe 2p XPS spectra of F-55-48 and T500-6 materials.

The positions of the satellite peaks for the Fe $2p_{1/2}$ and Fe $2p_{3/2}$ peaks were very sensitive to the oxidation states and these peaks had been used for qualitatively determining the ionic states of iron. Note that the XPS peak position of $Fe2p_{3/2}$ of F-55-48

and T500-6 samples was 711.08eV and 711.82eV, respectively. This information inferred the existence of Fe^{3+} in the catalysts.[3] Besides, the satellite peak position of Fe $2p_{1/2}$ was located at approximately 8eV higher than the main Fe $2p_{3/2}$ peak and this further identified the presence of Fe^{3+} in all samples.[4, 5]

S3.4 EPR characterization

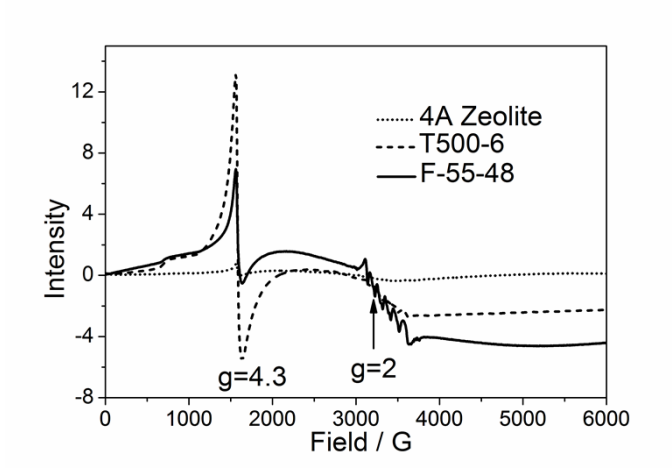

Fig. S7. The EPR spectra of 4A zeolite, F-55-48 and T500-6 catalyst.

In Fig.S7, EPR spectra of 4A zeolite, F-55-48 and T500-6 catalyst, which were measured at 90K, were compared. The spectra showed signals at effective g-values of 4.3 and 2.0, which have been found in a number of EPR studies on Fe-zeolites.[6-14] However, the assignment of these signals to certain iron species is still a matter of controversy,[9, 15] and the answer probably depends on the host zeolite structure used.[16] According to the literatures,[6-9, 11, 12, 14, 17] there is a distinguishing characteristic, the strong asymmetry of the signal at near g≈4.3, about exclusively isolated iron sites, as is shown in Fig. S8 (green line and red line, the axis of symmetry is set to zero based on the spin analysis of free electron[18]). Fig.S9 (77K, dashed line) is an example to explain the same observation which is reproduced with the permission from the reference[17]. In addition, it can be observed that the signal at near g≈4.3 presents good symmetry from the EPR spectra resulting from only iron oxides in solid matrix[19, 20] and so this may suggest that better symmetry means higher content of iron oxides in T500-6 material. Here it must be pointed out that the asymmetry of the signal at near g≈4.3 only can be observed from the spectroscopy measured at low temperature (<100K). In conclusion, it could be deduced that predominant amount of isolated iron species were in F-55-48 catalyst.

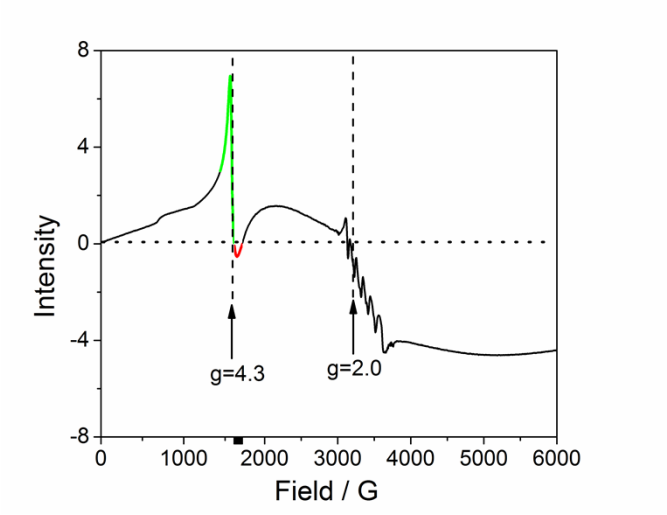

Fig. S8. The EPR spectra of F-55-48 catalyst.

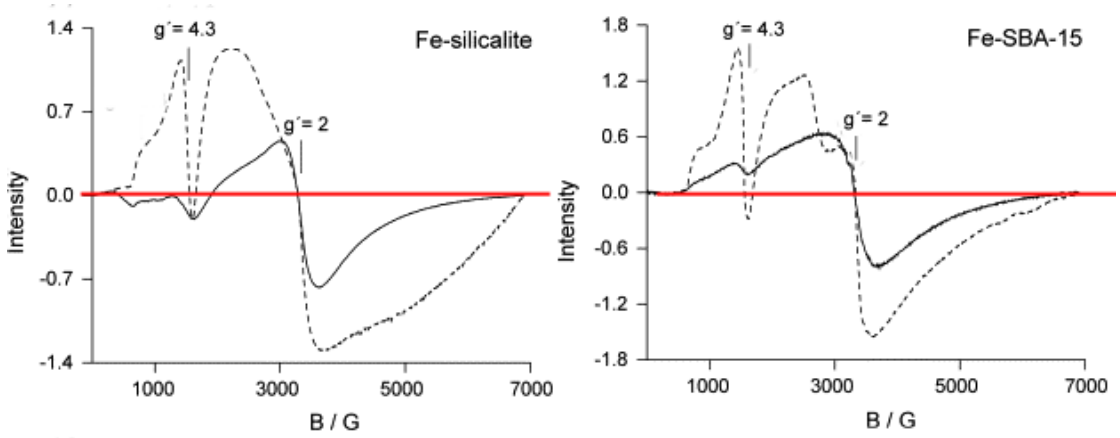

Fig.S9. EPR spectra of the catalysts measured at 77K (dashed line) and 298K (solid line). Adapted, with permission, from ref.18)

S3.5 The Al 2p deconvolution

Table S2. The Al 2p deconvolution for the calculation of $[AlO_4]$ and α-Al_2O_3 in catalysts.

Sample	Si/Al XPS (At. %/At. %)	Peak 1 $[AlO_4]$			Peak 2 α-Al_2O_3			$[SiO_4]/[AlO_4]$[b] (At. %/ At. %)
		Peak position (eV)	FWHM (eV)	$[AlO_4]$/total Al[f] (At. %/At. %)	Peak position (eV)	FWHM (eV)	α-Al_2O_3/total Al[a] (At. %/At. %)	
4A	1.052	73.75	1.63	100.000%	74.65	0	0	1.052
F-55-48	1.088	73.75	1.63	74.731%	75.65	1.65	25.269%	1.456
T500-6	1.219	73.75	1.63	5.241%	74.65	1.77	94.759%	23.259

Note: For comparison purposes, the coordination state of all the aluminum/silicon atoms in 4A zeolite was viewed as tetrahedral $[TO_4]$ (T=Si, Al) units. No aluminum/silicon oxides existed in zeolite. The deconvolution of Al 2p was executed according to the binding energy and FWHM of $[AlO_4]$ and α-Al_2O_3.

[a] [AlO_4]/total Al was obtained on the basis of the area ratio of [AlO_4] in total aluminum XPS area.

[b] [SiO_4]/ [AlO_4] was calculated according to the formula as follow:

$$\frac{[SiO_4]}{[AlO_4]} = (\frac{Si}{Al})/(\frac{[AlO_4]}{[total\ Al]})$$

S3.6 Existence state of [TO_4] (T=Si, Al)

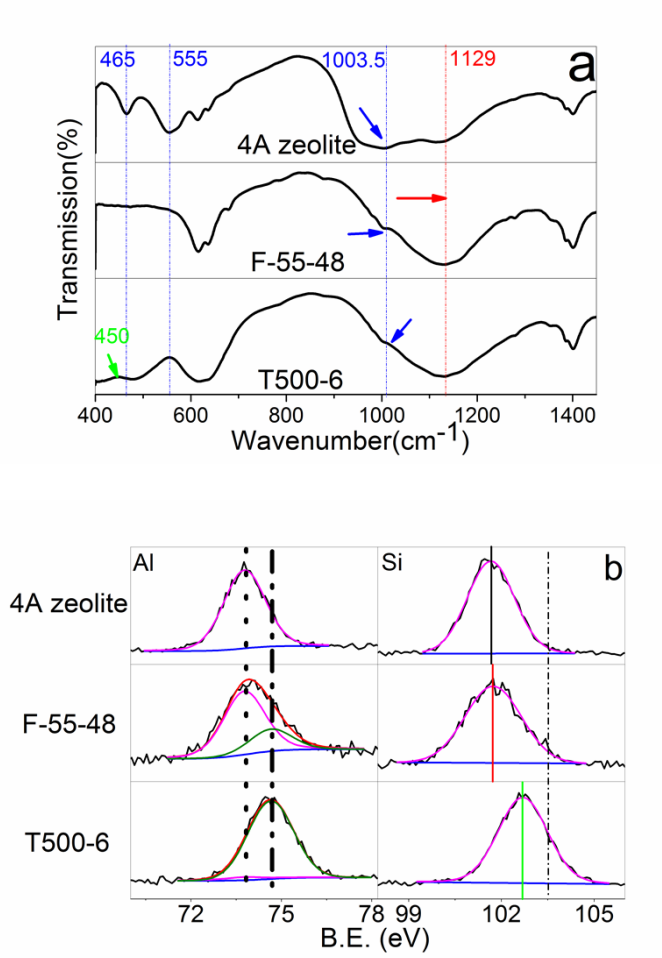

Fig. S10. a) The FTIR fingerprint and b) Al 2p and Si 2p XPS spectra of 4A zeolite, F-55-48 and T500-6 catalyst.

After we had good knowledge about iron species in different catalysts (Fig. 2), the structural properties of supporting materials needed be elaborated because of the importance of supports. In Fig.S2 and Fig.S3, 4A zeolite exhibited good crystalline structure, whereas F-55-48 and T500-6 catalysts almost completely lost their diffraction peak, so this outcome indicated that the structure properties of the 4A zeolite was destroyed after the iron was loaded on the zeolite. The infrared spectrum in the region of 400-1450cm^{-1} is a fingerprint of the region indicating structural features of frameworks and the spectrum was presented in Fig. S10a. With the IR spectrum comparison of 4A zeolite and iron-containing samples, one could find that the vibration band in the 465cm^{-1}

and 555cm^{-1} disappeared in iron-containing materials and this suggested the D4R units (S4 part) uniquely characteristic of LTA framework[21] was destroyed in the preparation of iron-loading catalysts. Also this destruction of D4R units gave the specific explanation why 4A zeolite underwent irreversible amorphization confirmed by XRD analysis above. Though the external linkages (D4R units) were destroyed, the internal [TO_4] (T=Si, Al) tetrahedral asymmetric stretching vibrations[22] in the region of 950cm^{-1}—1250cm^{-1} still existed. The strongest intensity at 1003cm^{-1} in 4A zeolite moved up to 1129cm^{-1} in iron-containing samples. This might be attributed to the increase of Si/Al ratio in tetrahedral sites[23] and the destruction of crystal structure. This phenomenon that only external linkages disappeared but internal [TO_4] tetrahedral units existed was similar to the structure destruction of LTA zeolite in high pressure[21] or temperature.[23] The gradual disappearance of the band at 1003cm^{-1} might evidence that the amount of [AlO_4] tetrahedrons in F-55-48 were more than that in T500-6 and the fact was confirmed in Table S2.

The Si 2p and Al 2p XPS spectra in Fig. S10b further provided detailed insight into the change of Si and Al coordination environment in supports. Accompanied with the iron species loading in zeolite, the binding energy of Si 2p and Al 2p shifted up to higher binding energy. One could find out that there was only subtle difference between 4A zeolite and F-55-48 in the binding energy of Si 2p and Al 2p (101.66eV vs 101.73eV, 73.77eV vs 74.02eV). Tery L.Barr pointed out that structural difference between zeolite Na-A and sodalite with Si/Al ≈ 1 may not be resolved by XPS, except perhaps as subtle shifts at very high resolution. Given that the structural affinity between 4A zeolite and sodalite (S4 part), we could reason that the structure of F-55-48 catalyst without any crystallinity became analogous to one of sodalite, i.e., 74.731% [AlO_4] (Table 1 and Table S2) and [SiO_4] primary building units still existed in F-55-48 samples. However, the binding energy of Al 2p in T500-6 catalysts reached up to 74.65eV which was in line with that in α-Al_2O_3[24] samples. The binding energy of Si 2p in T500-6 catalysts was 102.68eV corresponding to that in faujasite[25] but lower than that in SiO_2 (103.5eV)[26] or purely siliceous sodalite[27] (103.2eV). This gave the indication that [AlO_4] tetrahedrons were destroyed but [SiO_4] primary building units were held in incineration samples. It should be also noticed that not all [AlO_4] tetrahedrons were transformed into α-Al_2O_3 based on the lower binding energy of Si 2p in T500-6 materials than that in purely siliceous sodalite and the calculation ([AlO_4]/total Al atom =5.241%) as indicated in Table 1 or Table S2. Associated with the fact that the strongest asymmetric stretching intensity in aluminosilicate sodalite with SiO_2/Al_2O_3 ≈ 3.58[23] occurred at ca.1131cm^{-1}, one could understand that the structure of T500-6 materials also became analogous to the one of sodalite with higher Si/Al ratio. Based on the above analysis from vibrational spectrum, Scheme 1 to illustrate the propositional existence state of [TO_4] (T=Fe, Al and Si elements) units in different materials.

S4 The structure of LTA and SOD zeolite

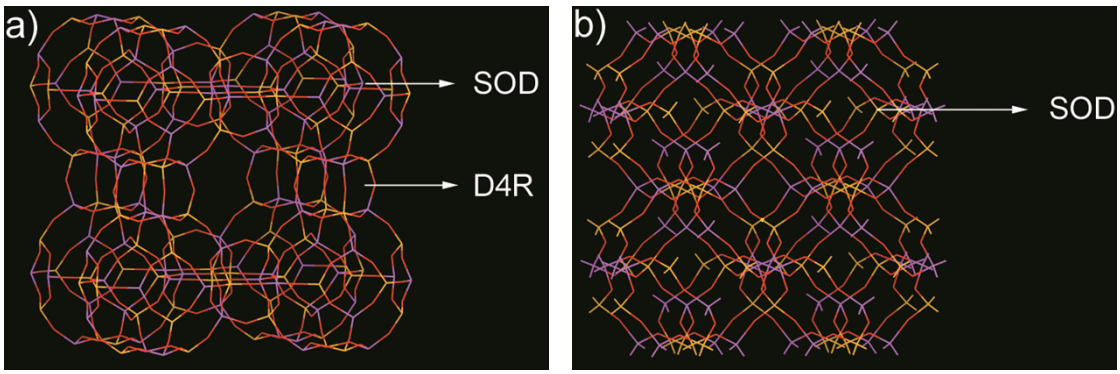

Fig. S11. The structure a) of 4A zeolite and b) of sodilate.

According to the Database of Zeolite Structures in International Zeolite Association, the structure 4A zeolite (one ITA units around 8 SOD and 8 D4R units) is made of 8 SOD and 8 D4R secondary structure units and solidate is composed of only 8 SOD units. After the D4R structure of LTA structure (as confirmed in Fig.10a IR spectra) was destroyed, the SOD might be hold in catalysts based on the analysis of the presence of tetrahedral structure. But the structure arrangement of tetrahedrons was random.

S5 The reason for zeolite structure breakdown in the catalyst preparation

Concerning the crystallographic degradation in Fe-exchanged zeolites, three reasons might be employed to explain the phenomenon: 1) Al^{3+}-Fe^{3+} exchange due to similar ionic radii and the same charge (high spin state Fe^{3+} ca. 0.645A Vs Al^{3+} ca. 0.535A); 2) the electronic unbalance caused by Na^{+}-Fe^{3+}(monovalent cation vs trivalent cation) exchanged; 3) the less intense structure resulted from the change of unit cell parameters after Na^{+}-Fe^{3+} exchange with different ionic radii (Na^{+} ca.1.02A Fe^{3+} ca. 0.645A).[28, 29]

S6 Catalytic performance

S6.1 pH buffer of F-55-48 and T500-6

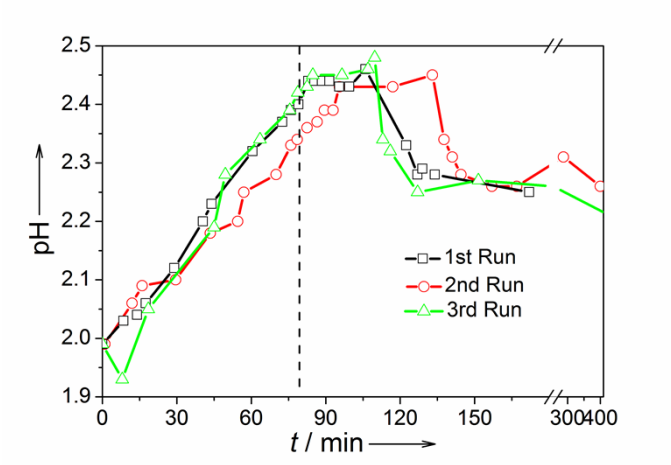

Fig. S12. The pH change of phenol solution in the presence of F-55-48 catalyst. Other conditions: phenol=200 mg/L, 100 mL; catalyst: 0.10 g; Initial pH=2.00±0.01; T=25°C. The black dashed line denotes the time when hydrogen peroxide is added to start the phenol reaction.

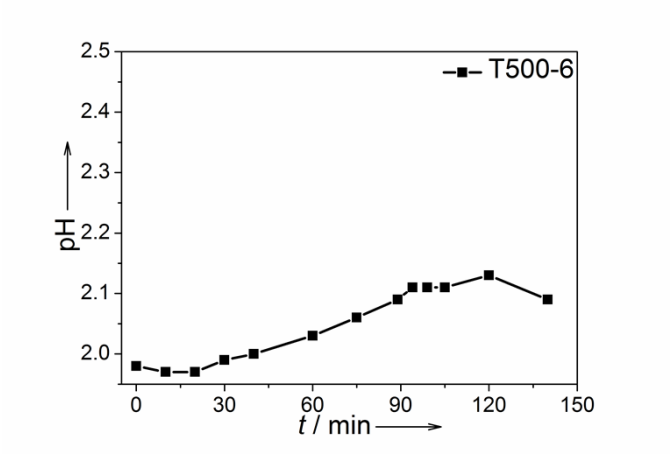

Fig. S13. The pH change of phenol solution in the presence of T500-6 catalyst. Other conditions: phenol=200 mg/L, 100 mL; catalyst: 0.10 g; initial pH=2.00; T=25°C.

S6.2 The mechanism of phenol degradation

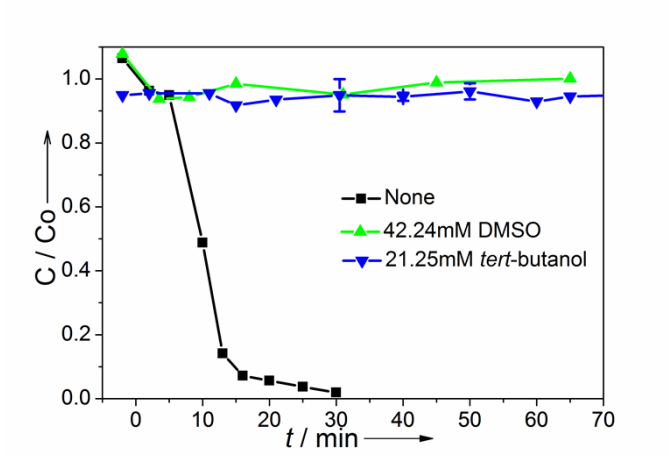

Fig. S14. Effect of *tert*-butanol and DMSO on phenol degradation with F-55-48 catalyst. Other conditions: Phenol=200 mg/L, 100 mL; H_2O_2/Phenol=12.75 (molar ratio); catalyst: 0.10 g; Initial pH=2.00±0.01; T=25°C

In Fig. S14, one could find out that excessive addition of *tert*-butanol or DMSO[30] would suppress completely phenol degradation in the presence of F-55-48 catalyst. This result indicated that hydroxyl radical plays an important role in phenol degradation, which was in agreement with Ma's opinion.[31]

The mechanism of radical quenching in Fenton reaction

Highly reactive hydroxyl radicals (HO·) are traditionally thought to be the main active species responsible for the destruction of the pollutants in Fenton reaction according to the classical Haber-Weiss mechanism.[32, 33] However, the hydroxyl radicals react non-selectively and immediately with solutes.[33, 34] The excessive addition of alcohols or some other scavengers[35-37] leads to the reaction of hydroxyl radicals with quenchers, and protects the probe molecule from degradation.

S6.3 The mechanism about shorter induction time of F-55-48 catalyst

About the origin of induction period in catalytic process, there are several explanations in literatures. First, it is thought as an activation process of the surface iron oxides, which are thus enabled to form complexes with the reactants (phenol and/or H_2O_2) before the oxidation process can occur.[38-40] Second, it is attributed to the protonation of the surface iron species (pH effect).[38, 41] Third, it is related to the hydroxyl radical-scavenging effect by the iron oxide and/or support.[37, 42, 43]

There is not a full consensus about the Fenton-like mechanism with supported iron species and this is related to the variation in the Fe coordination environment in diverse materials. According to the previous studies,[44-46] the mechanism of Fe^{3+} initiated Fenton-like reaction is summarized as follow:

$(Fe^{3+})\ s + H_2O_2 \rightarrow (H_2O_2)\ s$

$(H_2O_2)\ s \rightarrow (Fe^{2+})\ s + H_2O + HO_2\cdot$

(Fe^{2+}) s + H_2O_2 → (Fe^{3+}) s + ·OH

(Fe^{3+}) s and (Fe^{2+}) s represents the iron species with different valence state in solid matrix, while (H_2O_2) s denotes the formed H_2O_2 complex with iron species. In above equations, one can find that the production of hydroxyl radical must depend on the cycle of (Fe^{3+}) s and (Fe^{2+}) s. It may mean that the activation property of iron species will play a key role in Fenton-like reaction. In our catalytic system, the main difference of F-55-48 and T500-6 was the active species in each catalyst. It had been identified that predominant amount of isolated iron sites were in F-55-48 sample, while the iron oxides predominated in T500-6 materials. The tetrahedrally coordinated and atomically isolated $[MO_4]$ (M=Fe, Co, etc.) species play a more favourable role in catalysis than corresponding oxides.[47-52] So it is believed that the induction period is an activation process of iron species and F-55-48 catalyst show shorter induction period in phenol degradation than T500-6 sample.

S6.4 Phenol degradation under different pH conditions

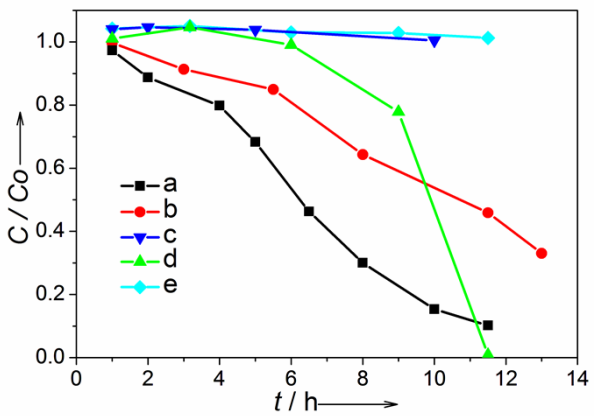

Fig. S15. Removal of phenol under different conditions: (a) 0.10 g F-55-48 and initial pH = 4.00; (b) 0.10 g F-55-48 and initial pH = 6.30; (c) 0.10 g T500-6 and initial pH = 5.00; (d) 0.10 g T500-6 and initial pH = 4.00; (e) 0.10 g T500-6 and initial pH = 6.30. Other reaction conditions: Phenol=200mg/L, 100mL; Catalyst=0.10 g; T=25°C; H_2O_2/Phenol=12.75 (molar ratio).

Fig. S15 exhibited phenol degradation under different pH condition. One could observe that, with pH being 4.00, almost all phenol was degraded at 11.5 h in the presence of F-55-48 or T500-6 catalyst. But phenol degradation was not observed with T500-6 catalyst when initial pH was 5.00 or 6.00, whereas about 60.00% phenol was destroyed with F-55-48 sample.

Although initial pH showed huge effect on Fenton reaction (Fig. 3a and Fig. S15), it was rather difficult to identify the true reasons about the pH effect on Fenton process. A further experiment would be clearly necessary on this point in our future researches. The factors that initial pH affected the Fenton catalytic activity would be listed afterwards.

The effect of pH on Fenton reaction

Concerning to pH effect on Fenton reaction, so many literatures has elaborated its vital role in this reaction process. After we summarize these literatures, the reason why higher pH is detrimental to Fenton catalytic activity is listed as follow:

① The oxidation potential of hydroxyl radical decreases at higher pH. The value ranges between 2.65 to 2.80V at pH 3.0 ant it lowers to 1.90V at pH 7.0;[53, 54]

② At higher pH values, the rapid H_2O_2 decomposition produces molecular oxygen without formation of appreciable amounts of hydroxyl radicals;[55-57]

③ The conversion of initial pH determines the establishment of pH_{pzc} (pH at the point of zero charge), and the synergistic effect of $pH_{terminal}$(terminal pH) and $pH_{pzc\ terminal}$ (terminal pH_{pzc})affects the density of surface hydroxyl groups in the neutral state, which controls the concentration of hydroxyl radical in Fenton process;[58]

④ High catalytic activity in low pH is ascribed to the surface activation through protonation[45] in non-radical mechanism of reaction;[59-61]

⑤ With iron oxides being the active sites, which can assume different forms according to the pH, the $Fe\text{-}OH_2^+$ will prevail at low pH whereas the $Fe\text{-}O^-$ form will dominate at high pH. The $Fe\text{-}OH_2^+$ form would be responsible for the H_2O_2 adsorption and fast catalytic rate in low pH.[45, 55, 59]

⑥ Under certain conditions, the iron leaching in low pH will be beneficial for fast Fenton reaction.[45, 62]

In conclusion, the pH effect on Fenton reaction is a very complex process. And it is rather difficulty to identify the true reasons about the pH effect on Fenton process. Anyway, a high pH is detrimental to Fenton catalytic activity.

In addition, it seems like that heterogeneous Fenton process displays stronger dependence on solution pH than homogeneous Fenton reaction.[44, 45, 63, 64] Active sites and components,[63] the property of support[65] and reaction conditions[44, 56, 64, 66, 67] are the key factors in heterogeneous process. So it is possible that solution pH showed the huge impact on the catalytic degradation of phenol at pH 2 and pH 4, but the real reason cannot be identified. A further experiment will be clearly necessary on this point in our future researches.

S6.5 H_2O_2 utilization efficiency of F-55-48 and T500-6 catalysts under specific conditions

Table S3. H_2O_2 efficiency of F-55-48 and T500-6 catalysts under specific conditions. Other conditions: Phenol=200mg/L, 100mL; Catalyst=0.10 g; T=25°C

pH	H_2O_2/Phenol	Efficiency [a] (%)	
		F-55-48	T500-6
2.00	1.28	76.94 (49.46[b])	54.62 (28.82[b])
2.00	6.38	38.55	18.27
4.00	12.75	12.00	8.37
5.00	12.75	10.13	No reaction
6.30	12.75	8.94	No reaction

[a] H_2O_2 efficiency is the ratio value of dissipative phenol and H_2O_2 (calculated by

equation 1). [b] H_2O_2 efficiency is obtained according to the literature.[68]

Equation 1: $E_{H_2O_2}\ (\%) = \frac{Po - P}{Ho - H} \times 100\%$ ..... (1)

In this equation, $E_{H_2O_2}$ (%) represents the H_2O_2 utilization efficiency. Po and P denote the initial and residual phenol amount (mol) at a specific time, respectively, while Ho and H refer to the initial and residual H_2O_2 amount (mol), respectively.

With initial pH≤3.00, the P and H was obtained based on the remnant concentration of phenol and hydrogen peroxide when the degradation reactions reached equilibrium. With initial pH≥4.00, the P and H was calculated according to the fitting equation of phenol and hydrogen peroxide degradation. The H_2O_2 efficiency was calculated when reaction time was 10h. Phenol degradation was fitted with pseudo first-order kinetic equation (the example was represented in Fig. S16).[69] Liner equation was used to fit the degradation of hydrogen peroxide (Fig. S17 is an exemplification). All R^2 value was more than 0.95.

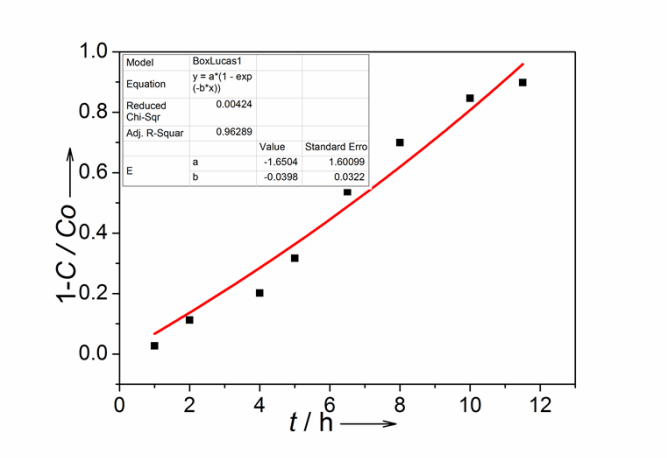

Fig. S16. The fitting of phenol degradation with pH=4.00.

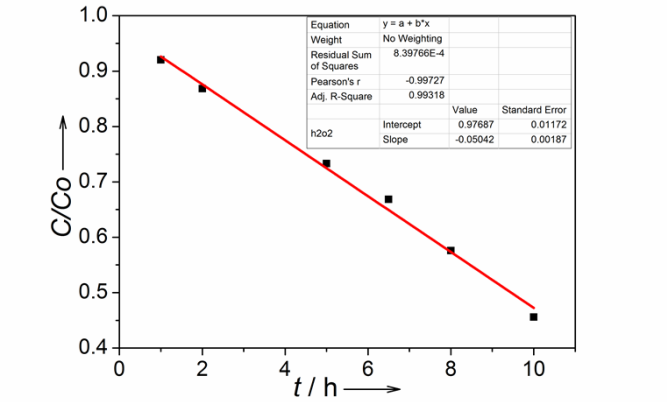

Fig. S17. The fitting of hydrogen peroxide degradation with pH=4.00.

S6.6 The effectiveness of lyophilization in catalyst preparation

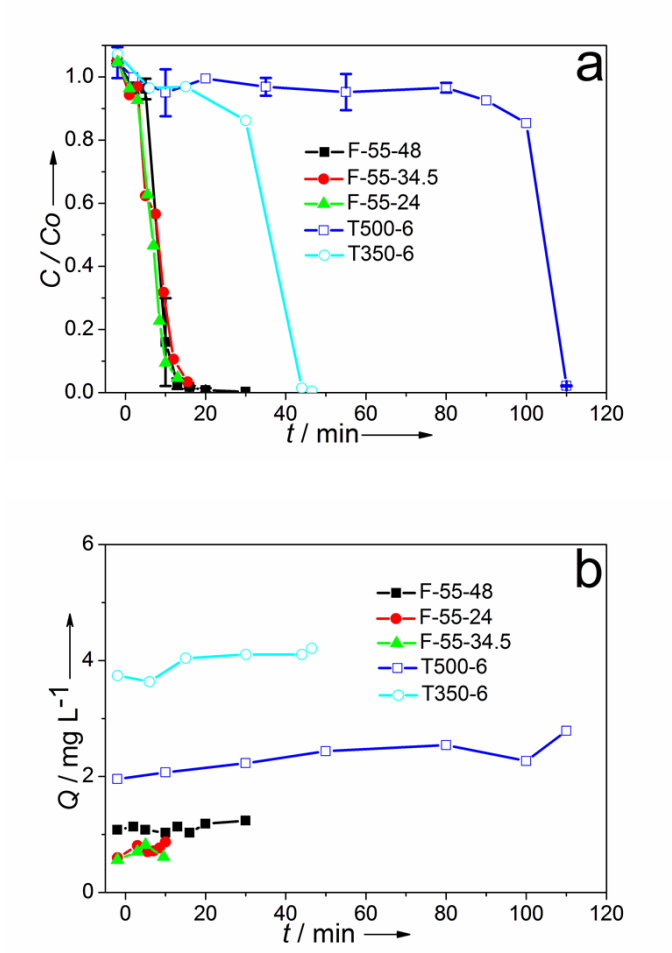

Fig. S18. a) Phenol degradation and b) iron leaching in the presence of different catalysts. Phenol=200 mg/L, 100 mL; H_2O_2/Phenol=12.75 (molar ratio); Catalyst=0.10 g; Initial pH=2.00±0.01; T=25 °C

S7 Catalysts prepared at room temperature

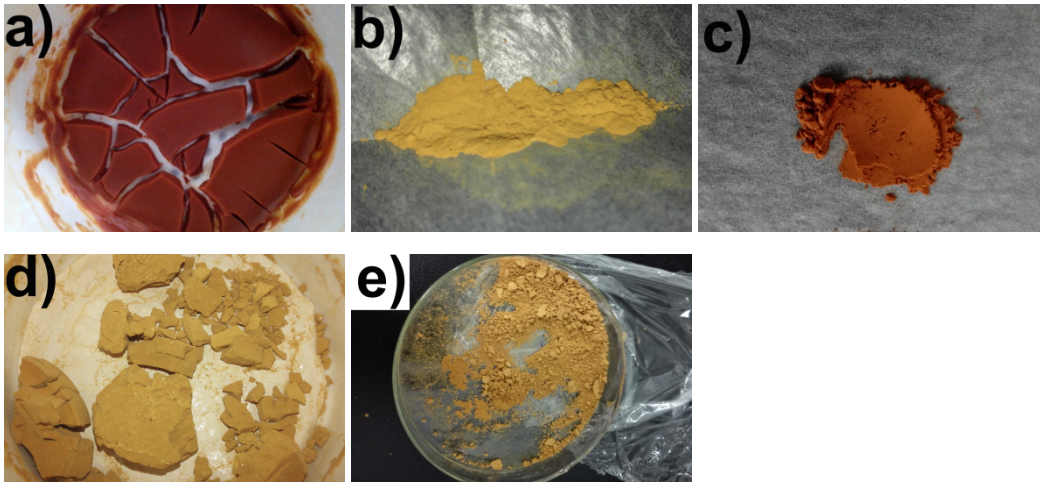

Fig.S18. The snapshot of a) catalyst precursor, b) F-55-48, c) T500-6, d) RT (dried for 30days at room temperature and pressure), and e) VT24 (dried for 24h under vacuum (-0.1MPa) at room temperature)

Fig.S18 presented the snapshot of as-prepared materials. It could be observed that large pieces were in RT samples (dried for 20days at room temperature and pressure) and large particles in VT24 materials (dried for 24h under vacuum (-0.1MPa) at room temperature), but only fine powder in F-55-48 and T500-6 catalysts. The reason for these results might be related to the dehydration rate in various preparation methods. Faster dehydration rate in lyophilization and calcination process led to fine powder. The measurements of particle size distribution indicated that the average diameter was 8.99μm for F-55-48 and 37.09μm for T500-6. To assess the catalytic performance of catalyst, the phenol degradation experiments in the presence of F-55-48 and RT catalyst were carried out and the snapshots at different time were presented in figure S19. After the addition of catalysts (0h), F-55-48 sample showed good dispersion but the RT catalyst had very bad dispersion. At 12h, RT catalyst showed better dispersion than 0h but one could still notice large particles in the bottom of the conical flask. The measurement of phenol concentration indicated that 64.45% phenol was degraded by F-55-48 but only 2.34% phenol disappeared for RT catalyst. If it was grinded into powder, the VT24 material still showed a chronic process for phenol degradation, as presented in Figure S20. The poor catalytic performance of VT24 and RT samples might result from the poor dispersion in reaction medium. So this fact further manifested the advantages of lyophilization in catalyst preparation.

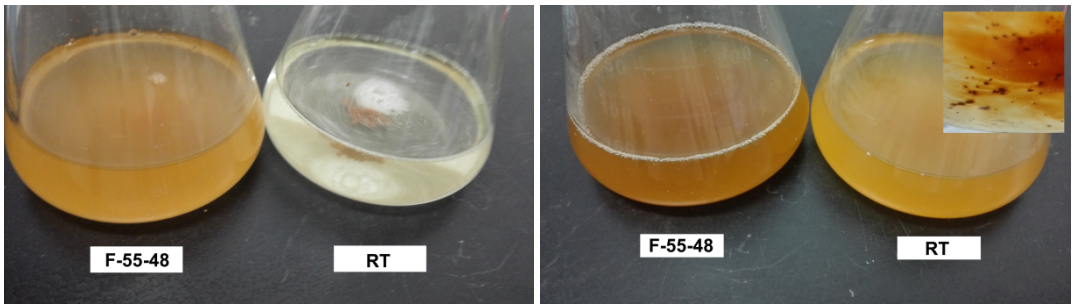

Fig.S19. The snapshot of left) 0h and right 12h) during phenol degradation with F-55-48 and RT catalysts (Inset: the view from the bottom of conical flask). Other conditions: Phenol=200 mg/L, 100 mL; H_2O_2/Phenol=12.75 (molar ratio); Catalyst=0.10 g; Initial pH=6.30; T=25 °C

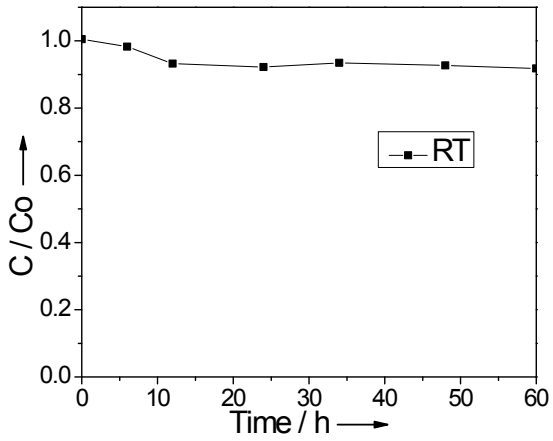

Fig.S20. Phenol degradation in the presence of VT24 catalyst. Phenol=200mg/L, 100mL; H_2O_2/Phenol=12.75 (molar ratio); Catalyst=0.10g; Initial pH=6.30; T=25°C

S8 The analysis of catalyst stability

Six successive recycling experiments are carried out at initial pH=6.30 and the results further show good stability of F-55-48 catalyst (Fig.3d).Compared with the freshly prepared sample, the SEM and TEM images in Fig. S21 showed that there was no change in the structure of F-55-48 catalyst after six successive recycling experiments. Similarly, the UV/Vis spectroscopy in Fig.S22 of the used catalyst showed subtle difference with the original sample. These data suggested the excellent stability of F-55-48 catalyst for phenol degradation in neutral pH.

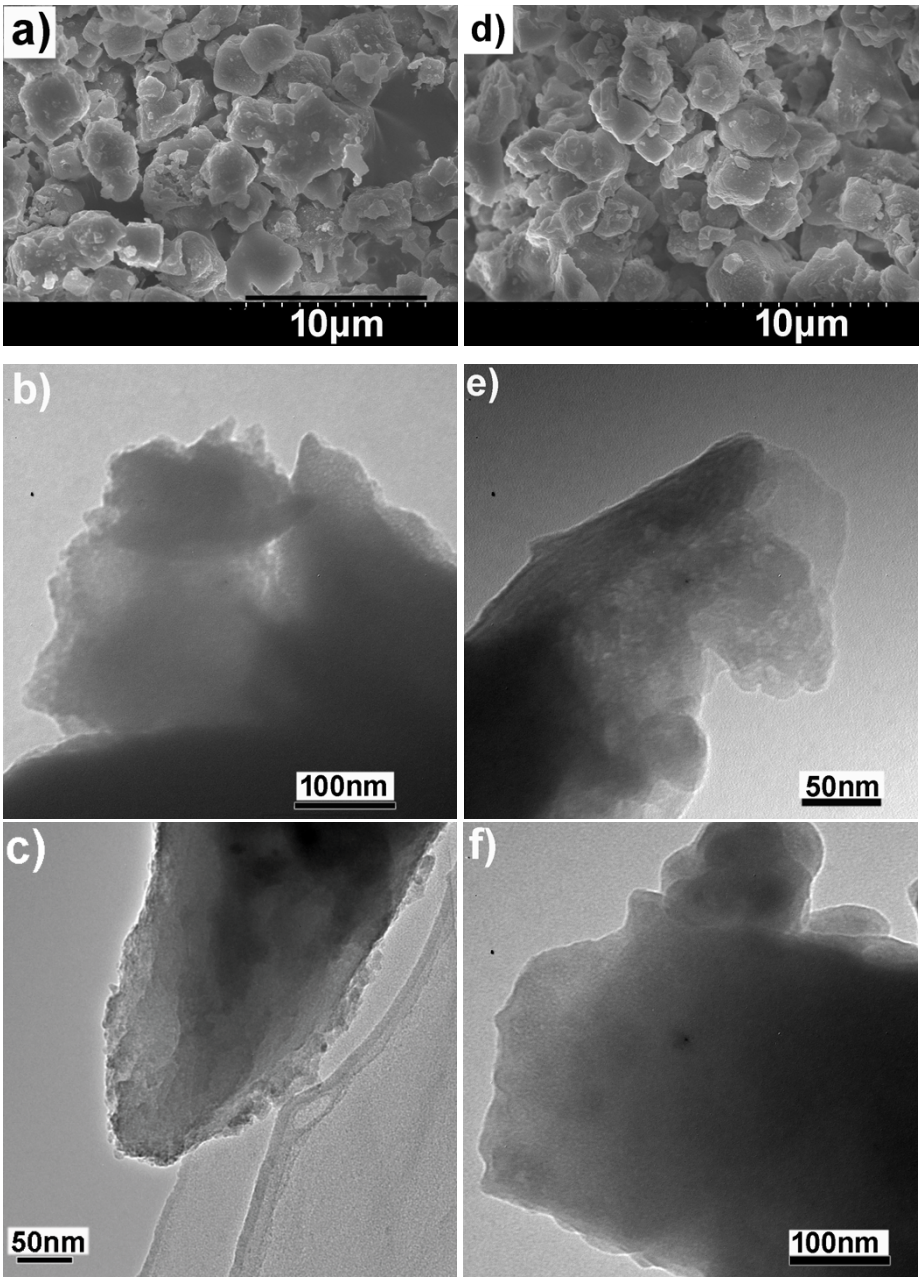

Fig.S21 The SEM images of a) before catalysis and d) after six cycles. The TEM images of b, c) before catalysis and e, f) after six cycles. Successive recycling experiments was carried out with F-55-48 catalyst at pH=6.30. Other conditions: Phenol=200 mg/L, 100 mL; H_2O_2/Phenol=12.75 (molar ratio); Catalyst=0.10 g; T=25 °C

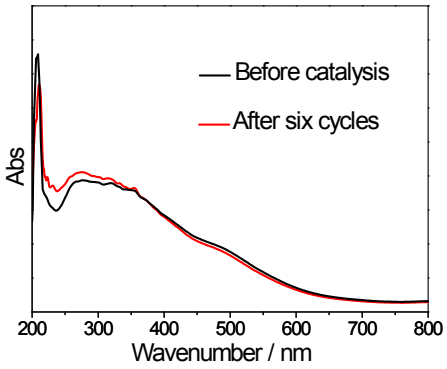

Fig. S22 The UV/Vis spectra of F-55-48 catalyst before catalysis and after six cycles. Successive recycling experiments was carried out with F-55-48 catalyst at pH=6.30. Other conditions: Phenol=200 mg/L, 100 mL; H_2O_2/Phenol=12.75 (molar ratio); Catalyst=0.10 g; T=25 °C

S9 Phenol adsorption

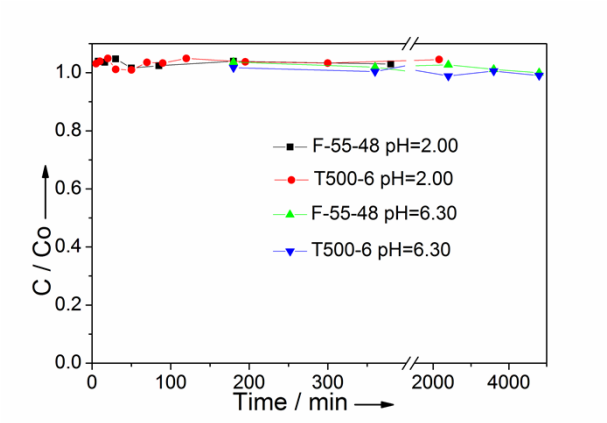

Fig.S23 Phenol adsorption as a function of time at different conditions. Other conditions: Phenol=200 mg/L, 100 mL; H_2O_2/Phenol=12.75 (molar ratio); Catalyst=0.10 g; T=25 °C

Fig.S23 showed that there was no phenol adsorption in F-55-48 and T500-6 catalysts regardless of the initial pH.

S10 Successive recycling performance

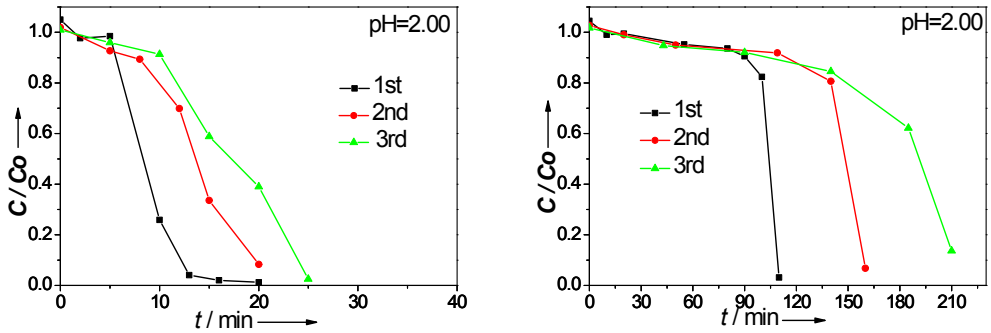

Fig.S24 Successive recycling experiments for phenol degradation in the presence of left) F-55-48 and right) T500-6 at initial pH=2.00. Other conditions: Phenol=200 mg/L, 100 mL; H_2O_2/Phenol=12.75 (molar ratio); Catalyst=0.10 g; T=25 °C

Fig.S24 showed successive recycling experiments of F-55-48 and T500-6 catalyst at initial pH=2.00. At pH=2.00, the time for the complete phenol degradation increased with the number of recycling experiments increasing, but the F-55-48 sample still showed slower activity decrease for phenol degradation than T500-6 one. This may be due to the more iron leaching of T500-6 in acid condition as evidenced in Fig. 3c. When initial pH was set to 6.30 (data not shown), the phenol concentration appeared no decrease at 12h in first experiment. After three successive tests, there was still little degradation for T500-6 catalyst (12h in each cycle). These data suggested that T500-6 had poorer stability for phenol degradation.

Reference

1 F. Chen, Y. Li, W. Cai and J. Zhang, *J. Hazard. Mater.*, 2010, **177**, 743.

2 R. M. Sellers, *Analyst*, 1980, **105**, 950.

3 R. M. Cornell and U. Schwertmann, *The iron oxides: structure, properties, reactions, occurrences and uses*, John Wiley & Sons, 2006.

4 A. Fujimori, M. Saeki, N. Kimizuka, M. Taniguchi and S. Suga, *Phys. Rev. B*, 1986, **34**, 7318.

5 M. Scrocco, *Phys. Rev. B*, 1981, **23**, 4381.

6 M. Schwidder, M. Santhosh Kumar, A. Brockner and W. Gronert, *Chem. Commun.*, 2005, 805.

7 M. Schwidder, M. Kumar, K. Klementiev, M. Pohl, A. Bruckner and W. Grunert, *J. Catal.*, 2005, **231**, 314.

8 M. Santhoshkumar, M. Schwidder, W. Grunert, U. Bentrup and A. Bruckner, *J. Catal.*, 2006, **239**, 173.

9 J. Perezramirez, J. Groen, A. Bruckner, M. Kumar, U. Bentrup, M. Debbagh and L. Villaescusa,

J. Catal., 2005, **232**, 318.
10 M. Mhamdi, S. Khaddar-Zine and A. Ghorbel, *Appl. Catal., A*, 2009, **357**, 42.
11 I. Ellmers, R. P. Vélez, U. Bentrup, A. Brückner and W. Grünert, *J. Catal.*, 2014, **311**, 199.
12 I. Ellmers, R. Pérez Vélez, U. Bentrup, W. Schwieger, A. Brückner and W. Grünert, *Catal. Today*, 2015.
13 P. Boroń, L. Chmielarz and S. Dzwigaj, *Appl. Catal., B*, 2015, **168-169**, 377.
14 E. Berrier, O. Ovsitser, E. Kondratenko, M. Schwidder, W. Grunert and A. Bruckner, *J. Catal.*, 2007, **249**, 67.
15 D. Goldfarb, M. Bernardo, K. G. Strohmaier, D. E. W. Vaughan and H. Thomann, *J. Am. Chem. Soc*, 1994, **116**, 6344.
16 E. A. Zhilinskaya, G. Delahay, M. Mauvezin, B. Coq and A. Abouka07s, *Langmuir*, 2003, **19**, 3596.
17 M. S. Kumar, J. Pérez-Ramírez, M. N. Debbagh, B. Smarsly, U. Bentrup and A. Brückner, *Appl. Catal., B*, 2006, **62**, 244.
18 M. Kaupp, M. Bühl and V. G. Malkin, *Calculation of NMR and EPR parameters: theory and applications*, John Wiley & Sons, 2006.
19 G. Ennas, A. Musinu, G. Piccaluga, D. Zedda, D. Gatteschi, C. Sangregorio, J. L. Stanger, G. Concas and G. Spano, *Chem. Mater.*, 1998, **10**, 495.
20 P. V. Finotelli, M. A. Morales, M. H. Rocha-Leão, E. M. Baggio-Saitovitch and A. M. Rossi, *Mater. Sci. Eng., C*, 2004, **24**, 625.
21 E. A. H. Yinning Huang, *Chem. Phys. Lett.*, 2001, **345**, 65.
22 M. K. Włodzimierz MOZGAWA, Katarzyna BARCZYK, *CHEMIK*, 2011, **7**, 667.
23 M. F. Edith and B. S. Leonard, *Molecular Sieve Zeolites-I*, AMERICAN CHEMICAL SOCIETY, 1974.
24 P. H. Bolt, E. ten Grotenhuis, J. W. Geus and F. H. P. M. Habraken, *Surf. Sci.*, 1995, **329**, 227.
25 T. L. Barr, *Appl. Surf. Sci.*, 1983, **15**, 1.
26 J. G. Yu, H. G. Yu, B. Cheng, X. J. Zhao, J. C. Yu and W. K. Ho, *J. Phys. Chem. B*, 2003, **107**, 13871.
27 H. H. Bruno Herreros, Tery L. Barr, and Jacek Klinowski, *J . Phys. Chem.*, 1994, **98**, 1302.
28 E. Díaz, S. Ordóñez, A. Vega and J. Coca, *J. Chromatogr. A*, 2004, **1049**, 161.
29 E. Asedegbega-Nieto, E. Díaz, A. Vega and S. Ordóñez, *Catal. Today*, 2010, **157**, 425.
30 S. Enami, Y. Sakamoto and A. J. Colussi, *PNAS*, 2014, **111**, 623.
31 L. W. Chen, J. Ma, X. C. Li, J. Zhang, J. Y. Fang, Y. H. Guan and P. C. Xie, *Environ. Sci. Technol.*, 2011, **45**, 3925.
32 J. Herney-Ramirez, M. A. Vicente and L. M. Madeira, *Appl. Catal., B*, 2010, **98**, 10.
33 E. Neyens and J. Baeyens, *J. Hazard. Mater.*, 2003, **98**, 33.
34 M. Pera-Titus, V. Garćıa-Molina, M. A. Baños, J. Giménez and S. Esplugas, *Appl. Catal., B*, 2004, **47**, 219.
35 S. Navalon, M. Alvaro and H. Garcia, *Appl. Catal., B*, 2010, **99**, 1.
36 P. Bautista, A. F. Mohedano, J. A. Casas, J. A. Zazo and J. J. Rodriguez, *J. Chem. Technol. Biotechnol.*, 2008, **83**, 1323.
37 A. L.-T. Pham, C. Lee, F. M. Doyle and D. L. Sedlak, *Environmental science & technology*, 2009, **43**, 8930.
38 M. Luo, D. Bowden and P. Brimblecombe, *Appl. Catal., B*, 2009, **85**, 201.

39 M. Timofeeva, S. T. Khankhasaeva, S. Badmaeva, A. Chuvilin, E. Burgina, A. Ayupov, V. Panchenko and A. Kulikova, *Appl. Catal., B*, 2005, **59**, 243.

40 A. S. Goldstein, R. H. Beer and R. S. Drago, *J. Am. Chem. Soc*, 1994, **116**, 2424.

41 J. T. Groves and Y. Watanabe, *J. Am. Chem. Soc*, 1988, **110**, 8443.

42 C. M. Miller and R. L. Valentine, *Water Res.*, 1999, **33**, 2805.

43 H. Ohkita, R. Nishiyama, Y. Tochihara, T. Mizushima, N. Kakuta, Y. Morioka, A. Ueno, Y. Namiki and S. Tanifuji, *Ind. Eng. Chem. Res.*, 1993, **32**, 3112.

44 L. Xu and J. Wang, *Environ. Sci. Technol.*, 2012, **46**, 10145.

45 N. Inchaurrondo, J. Font, C. P. Ramos and P. Haure, *Appl. Catal., B*, 2016, **181**, 481.

46 C. K. Duesterberg, S. E. Mylon and T. D. Waite, *Environ. Sci. Technol.*, 2008, **42**, 8522.

47 Y. Sun, S. Gao, F. Lei and Y. Xie, *Chem. Soc. Rev.*, 2015, **44**, 623.

48 S. Yashnik and Z. Ismagilov, *Appl. Catal., B*, 2015, **170–171**, 241.

49 Y. Wang, Q. Zhang, T. Shishido and K. Takehira, *J. Catal.*, 2002, **209**, 186.

50 G. Zhang, J. Long, X. Wang, Z. Zhang, W. Dai, P. Liu, Z. Li, L. Wu and X. Fu, *Langmuir*, 2009, **26**, 1362.

51 Y. Meng, H. C. Genuino, C.-H. Kuo, H. Huang, S.-Y. Chen, L. Zhang, A. Rossi and S. L. Suib, *J. Am. Chem. Soc.*, 2013, **135**, 8594.

52 J. Janas, T. Machej, J. Gurgul, R. P. Socha, M. Che and S. Dzwigaj, *Appl. Catal., B*, 2007, **75**, 239.

53 A. A. Burbano, D. D. Dionysiou, M. T. Suidan and T. L. Richardson, *Water Res.*, 2005, **39**, 107.

54 G. V. Buxton, C. L. Greenstock, W. P. Helman and A. B. Ross, *J. Phys. Chem. Ref. Data*, 1988, **17**, 513.

55 M. L. Kremer, *J. Phys. Chem. A*, 2003, **107**, 1734.

56 J. Ramirez, F. Maldonado-Hódar, A. Pérez-Cadenas, C. Moreno-Castilla, C. Costa and L. Madeira, *Appl. Catal., B*, 2007, **75**, 312.

57 F. Duarte, F. Maldonado-Hódar, A. Pérez-Cadenas and L. M. Madeira, *Appl. Catal., B*, 2009, **85**, 139.

58 L. Zhao, J. Ma, Z. Sun and X. Zhai, *Environ. Sci. Technol.*, 2008, **42**, 4002.

59 R. Andreozzi, M. Canterino, V. Caprio, I. Di Somma and R. Marotta, *J. Hazard. Mater.*, 2008, **152**, 870.

60 F. Buda, B. Ensing, M. Gribnau and E. J. Baerends, *Chem. Eur. J.*, 2001, **7**, 2775.

61 B. Ensing, F. Buda and E. J. Baerends, *J. Phys. Chem. A*, 2003, **107**, 5722.

62 W. M. Wang, J. Song and X. Han, *J. Hazard. Mater.*, 2013, **262**, 412.

63 S.-h. Lee, J.-y. Oh and Y.-c. Park, *Bull. Korean Chem. Soc.*, 2006, **27**, 489.

64 E. M. Rodríguez, G. Fernández, P. M. Álvarez, R. Hernández and F. J. Beltrán, *Appl. Catal., B*, 2011, **102**, 572.

65 C. M. Yim, C. L. Pang, D. R. Hermoso, C. M. Dover, C. A. Muryn, F. Maccherozzi, S. S. Dhesi, R. Pérez and G. Thornton, *PNAS*, 2015, **112**, 7903.

66 B. G. Kwon, D. S. Lee, N. Kang and J. Yoon, *Water Res.*, 1999, **33**, 2110.

67 A. A. Burbano, D. D. Dionysiou, M. T. Suidan and T. L. Richardson, *Water Res.*, 2005, **39**, 107.

68 S. Li, G. Li, G. Li, G. Wu and C. Hu, *Microporous Mesoporous Mater.*, 2011, **143**, 22.

69 H. Lim, J. Lee, S. Jin, J. Kim, J. Yoon and T. Hyeon, *Chem. Commun.*, 2006, 463.